NDT&E International 148 (2024) 103221

Contents lists available at ScienceDirect

NDT and E International

journal homepage: www.elsevier.com/locate/ndteint

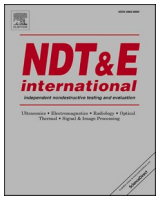

Machine learning based approach for automatic defect detection and classification in adhesive joints

Damira Smagulova [a,b,*], Vykintas Samaitis [a], Elena Jasiuniene [a,b]

[a] Prof. K. Baršauskas Ultrasound Research Institute, Kaunas University of Technology, K. Baršausko str. 59, LT-51423, Kaunas, Lithuania
[b] Department of Electronics Engineering, Kaunas University of Technology, Studentu st. 50, LT-51367, Kaunas, Lithuania

ARTICLE INFO

Keywords:
Ultrasonic testing
Machine learning
Interface defects
Adhesive joints
Defect characterization

ABSTRACT

This study presents an automated technique combining ultrasonic pulse echo method with machine learning algorithms to detect and classify the depth of interface defects in adhesively bonded joints. After data pre-processing for machine learning and extracting 32 ultrasonic features, the binary and ternary datasets were established for "defect"-"no defect" and its depth classifications. The importance and classification accuracy of various feature subsets—initial, single interface, minimised, tree-based, recursive, sequential, and LDA—were explored. A support vector machine (SVM) model was trained on these datasets. For "defect" vs. "no defect" classification, the initial feature subset achieved over 90 % accuracy on train/test data and 83 % on unseen data. For the ternary dataset, depth classification accuracy on unseen data in recursive feature subset was 97 % for "depth 1," 62 % for "depth 2," and 91 % for "depth 3." The obtained results demonstrate prediction accuracy and suitability of ML models for classifying defects and predicting their depths in adhesive bonds.

1. Introduction

Over the decades, the performance requirements of materials and structures in various industrial applications have grown with the advancement of science [1]. Adhesive joining technology is a fairly new technology that is an alternative to common joining methods such as welding, soldering, riveting, and mechanical fastening [2,3]. Adhesive joints are very attractive structures to such industries as aerospace, marine, automotive, wind power and others due to simplicity and low cost of their production and assembly, ability to join dissimilar materials, advanced mechanical characteristics and other properties [2,4–6]. The use of adhesive joints in the aerospace industry is very promising as it can significantly reduce the weight of the structure, reduce the carbon dioxide emission, and guarantee superior mechanical performance. Thus, adhesive bonding of metals, composites, or their hybrid are energetically more efficient [7].

However, structural integrity can be compromised at various stages, during the fabrication of structures, its preparation and bonding process, and in service. The weakest area in such structures is the bonding area which can be damaged by contamination, applied loads or environmental effects [2]. Common defects which occur in adhesive interface are delaminations, disbonds, voids, porosity and, in addition there can be weak or kissing bonds. All these defects are not visible and are in the interface between the two bonded materials. Ultrasonic inspection is one of the most reliable nondestructive testing (NDT) methods that is used to examine adhesively bonded joints. However, to locate such defects as disbonds and delaminations in multilayered dissimilar structures is still very challenging task because of influence of acoustic properties of the materials which can affect the propagation of ultrasonic waves. In addition, acoustic impedance mismatch at structure interfaces can cause reflections and mode conversions of the ultrasonic signals what complicates the detection of defects. Ultrasonic testing is an attractive and reliable method for identification of interface defects in multilayered structures, but high-quality control requirements are applied in the aerospace industry. For adhesive joints to be widely used, inspection method reliability, optimization and automatization must be guaranteed [3,8–10].

At the moment, a lot of research is being done in this field on increasing the reliability and performance of the method of controlling bonding integrity in adhesive joints. There are many nondestructive inspection techniques [10–12], numerical modeling [13–15], qualitative evaluations [16] and post-processing algorithms. Crane et al. [10] discussed such NDI techniques as ultrasonic methods, transient thermography and shearography capable of detecting adhesive joint defects.

* Corresponding author. Prof. K. Baršauskas Ultrasound Research Institute, Kaunas University of Technology, K. Baršausko str. 59, LT-51423, Kaunas, Lithuania.
E-mail address: damira.smagulova@ktu.lt (D. Smagulova).

https://doi.org/10.1016/j.ndteint.2024.103221
Received 13 June 2024; Received in revised form 23 August 2024; Accepted 25 August 2024
Available online 27 August 2024

Different approaches of ultrasonic testing of adhesive joints along with the development of post-processing algorithm techniques for reconstruction of the joined area which is under interest are being proposed [3,4,9,11,16–20]. Moreover, there are a number of studies which involve ultrasonic guided waves for assessing quality of adhesive connections. The principle of this method is that the wave field carries important information about the anomalies in the structure after guided waves interact with defects in adhesive joints [21–24]. In addition, defects of adhesively bonded joints were studied using laser ultrasound by generating shear waves for defect imaging [25], electromechanical impedance spectroscopy where mechanical impedance change occurs around the defect [26], evaluation of the resonance frequencies (Fokker bond test) to characterize the bonded structure [27] and others.

Our previous work was focused on the improvement of the ultrasonic inspection technique reliability. Techniques to increase probability of interface defect detection in adhesively bonded structures of similar and dissimilar materials were developed including elimination of influential factors on the detectability using developed post-processing algorithms, extraction of high-performance ultrasonic (UT) features, and extracting the information from the multiple reflections [4,16]. However, these techniques are time-consuming and require the evaluation of data by a professional expert. In terms of optimizing and automation such inspection techniques artificial intelligence (AI) is a very attractive solution. Today, its study is on the rise and its application is being found in various fields.

In the past, AI was mostly applied in the NDT field as knowledge based expert systems. The expertise is encoded into the rules of these systems in order to make the decisions regarding the state of the sample under investigation [28]. Recently, Prakash et al. [29] proposed machine learning (ML) algorithms for defect detection in fiber metal laminate structures from ultrasonic scans. This method includes image feature extraction and various classifiers which are used to distinguish defects in the ultrasonic scans. The HoG-Linear SVM classifier showed a better performance compared to SURF-Decision Fine Tree for determination of such defects as porosity, fold, twist, gap and inclusions [29]. Chen et al. [30] developed backpropagation neural network (NN) to analyze and predict porosity defects of various levels in composites. Computed tomography (CT) results were used to train and validate the NN model while the ultrasonic feature results were used as input signals. As a result, the porosity level in composites is predicted by the NN algorithm and compared to CT results [30]. Deep denoising NN model was constructed to characterize inclined cracks in noisy environments based on scattering matrix (interaction between ultrasonic waves and defects) and Bayesian inversion approach by Guo et al. [31]. Scattering matrix denoising network (SMDNet) consists of two networks of noise estimation and denoising. Noise estimation network takes as an input noisy scattering matrix and evaluates noise maps. Denoising network takes as an input noisy scattering matrix and noise maps to obtain noise-free scattering matrix of defect. This approach is useful for detecting crack defects with large angular orientations and can reduce the uncertainty in defect characterization [31]. Rao et al. [6] quantitatively reconstructed high-contrast disbond type defects in multi-layered bonded composites by using ultrasonic testing to collect data, which was then processed with a fully convolutional network (FCN) for detailed analysis. Tunukovic et al. [32] proposed the method of automated NDE to reduce interpretation time of ultrasonic data and minimize possibility of human error. The method consists of an intelligent gating process using density-based spatial clustering and noise clustering methods; and autoencoder (AE) to detect defects which is trained with non-defective ultrasonic data [32]. Two approaches were compared to classify the bonding state in adhesively bonded thermoplastic composites such as physics-based statistical method and machine learning based on SVM algorithm by Li et al. [33]. The machine learning approach showed higher accuracy in classification and is suggested to be used in complex composites and structures which are bonded adhesively [33]. Fu et al. [34] detected damages with greater accuracy in composite materials using laser ultrasound technology and artificial three-layer neural network (ANN). The study of Samaitis et al. [35] investigated the detection of weak bonds in adhesively bonded aluminium joints using linear ultrasound and machine learning algorithms. The data were analyzed using various feature selection techniques and support vector machine (SVM) classifiers where linear discriminant analysis (LDA) feature selector demonstrated a good balance between sufficient classification accuracy and about 40 % improvement in training time [35]. Despite the already existing contributions made in the field of adhesive bonding research and increasing the reliability of non-destructive inspection techniques and methods, this field remains to be challenging and needs to be explored, also with the application of artificial intelligence, in order to achieve high efficiency and reliability to meet the requirements in the aviation industry.

The goal of our study is to develop automated technique based on ultrasonic NDE and machine learning algorithms in order to detect and classify according to depth disbond and delamination type defects in adhesively bonded aluminium to composite materials with higher accuracy, increased measurement speed and repeatability and minimised human error. To achieve this goal two samples of adhesively bonded aluminium to carbon fibre reinforced plastic (CFRP) with interface defects were investigated using ultrasonic NDT technique. The experimental data was collected and preprocessed to eliminate major influential factors, enhance signal quality, identify specific time intervals, and extract 32 ultrasonic features that characterize the bonding state of the samples. For the automatization of the defect detection and depth classification technique the machine learning algorithms were developed based on feature engineering, dimensionality reduction techniques and SVM classifier used for training and accuracy evaluation.

2. Materials & methods

In this section the methodology of investigation of adhesively bonded joints and data preparation for machine learning model training is described. It comprises objects description, data acquisition, data preprocessing and development of machine learning algorithms. Two different specimens of bonded aluminium to CFRP were used for this research. Data from one sample was used for training of machine learning model, another sample was used to receive “unseen” data in order to evaluate performance of the model. Both objects were investigated using ultrasonic bulk waves and resultant data was collected. The next step was to preprocess collected data for the machine learning training and establish SVM classifiers for different feature subsets to evaluate defect classification accuracy. Workflow schematic is shown in Fig. 1.

2.1. Objects description

Objects under investigation were two adhesively bonded aluminium to carbon fibre reinforced plastic (CFRP) joints manufactured by global aircraft maintenance and repair company FL Technics in Lithuania. There are 9 artificial interface defects of rectangular shape with dimensions of 15 mm, 10 mm and 5 mm in each sample. To glue aluminium and CFRP plates two adhesive films Scotch Weld AF163-2K were used. Double-folded rectangular pieces of solid film A5000RED were used to create disbond and delamination type defects. Double-folded solid films of 3 different sizes were placed between aluminium plate and adhesive film forming disbonds, another 3 pieces were placed between 2 layers of adhesive films forming delaminations; and last 3 pieces of film inserted between adhesive tape and CFRP. Thus, the defects are located at different depths of the interface. The sample with thin CFRP plate was used for training and testing data, the sample with thick CFRP plate was used to collect “unseen” data. Schematics of both samples under investigation are shown in Fig. 2.

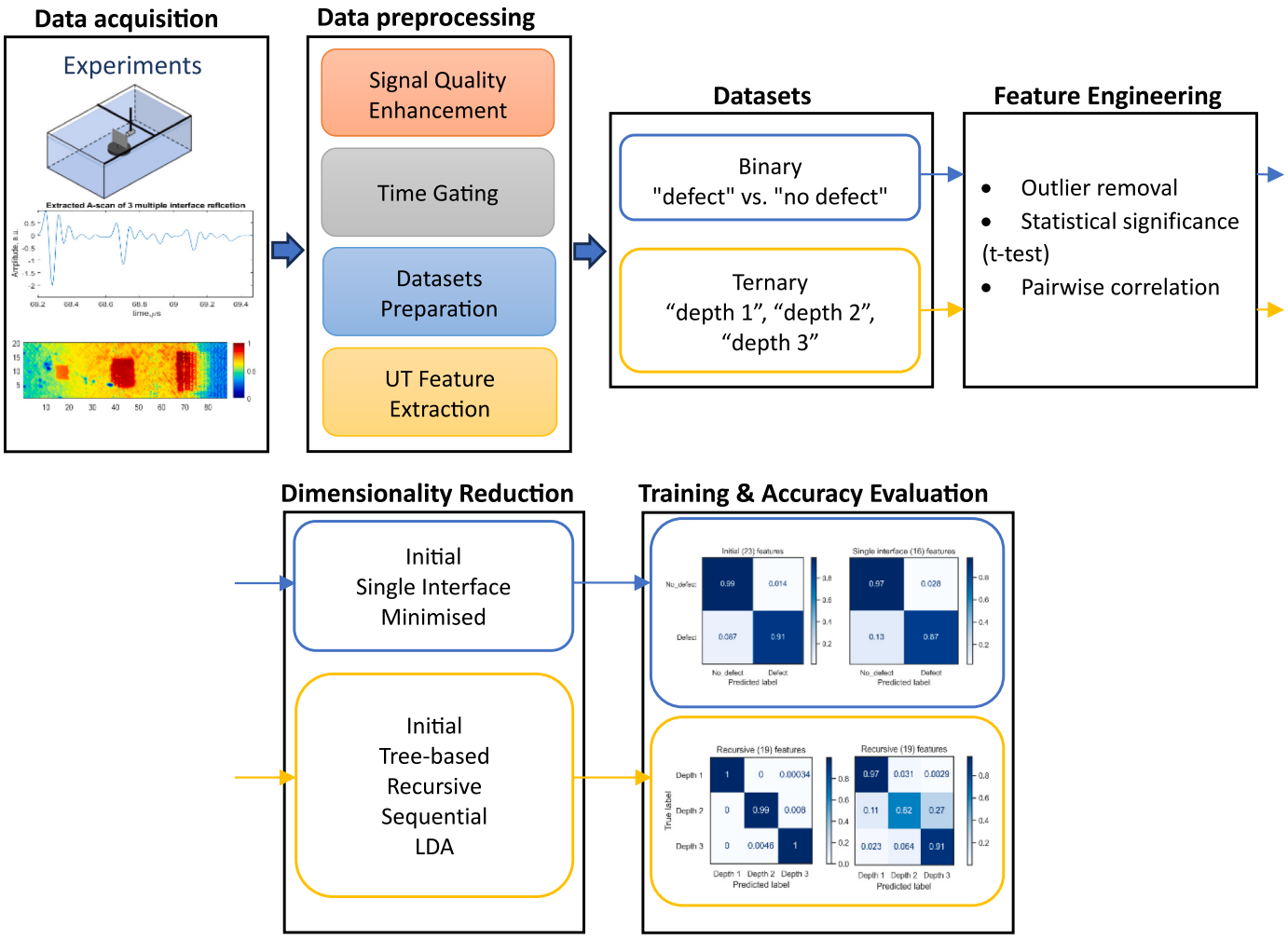

Fig. 1. Workflow schematic of the automatic defect detection and classification.

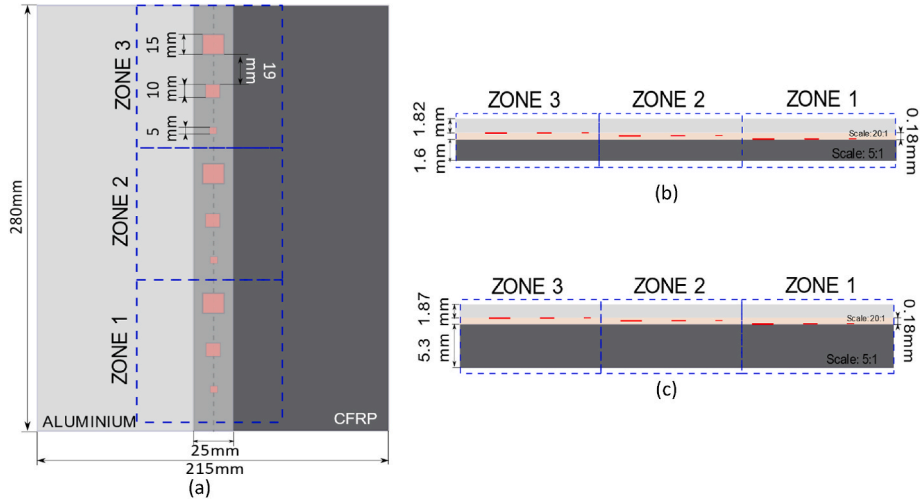

Fig. 2. Schematics of adhesively bonded aluminium to CFRP joints: (a) top view of both samples; (b) front view of sample No 1; (c) front view of sample No 2.

2.2. Ultrasonic NDE

Pulse echo immersion ultrasonic technique was used to conduct experimental investigation of the adhesively bonded joints. 15Mhz focused transducer with the sample were immersed into the tank filled with water. TecScan measurement system was used for the investigation where the scanning step was set to 0.2 mm, sampling rate to 200Mhz and the gain was 11 dB for sample No 1 and 17 dB for sample No 2,

respectively.

While preparing the objects for scanning it was discovered that they were slightly bent. In sample No 1, it is possible to observe that the sample is bent visually. In the case of specimen No 2, the curvature cannot be seen visually, but it is present and is detected by the time delay difference comparing ultrasonic signals reflected from the object surface. Even this slight curvature is a significant factor that affects the detectability of adhesive defects [16]. Because the samples were not planar, the scanning zone was divided into 3 zones (Fig. 2) in order to properly align the transducer. The transducer was positioned perpendicularly to the surface of the object under testing to maximize the amount of reflected energy from the surface of the object. The ultrasonic scanning of the object was performed in the z and y axes directions. The experimental set-up of the investigation is shown in Fig. 3.

2.3. Data preprocessing for machine learning

The data preprocessing stage is crucial in ensuring the quality and reliability of the training dataset, ultimately influencing the accuracy and effectiveness of the defect detection technique. Main data preprocessing steps applied on the signal A-scans are shown in Fig. 4. Enhancement of signal quality was performed to increase signal-to-noise ratio, time gating was applied to extract signal segments critical for defect detection, specific data were selected from defected and not defected areas and ultrasonic features were determined and extracted for further machine learning.

2.3.1. Enhancement of the signal quality and relevance

In order to enhance the signal-to-noise ratio and improve the visibility of defect-related information, bandpass filtering was applied to the collected data. Another procedure to improve interface defect detection in the specimens is to perform time alignment of the reflected ultrasonic signals from the surface. It has been proven in our work [16] that the curvature of the specimen, which is not even visible visually, is a huge factor affecting the probability of defect detection. Due to the curvature of the surface of the object, the time of propagation and reflection of ultrasonic waves from it is different. Therefore, when analyzing signals related to the adhesive layer where the defects are located, this factor complicates detection. By eliminating this factor, it is possible to greatly increase the detectability of defects. This procedure is based on the zero-crossing technique, where the arrival time of the signals is aligned by determining the time interval by which the signals should be shifted.

2.3.2. Time gating of the signal

The next step in preparing the signal for machine learning is to determine the time intervals on ultrasonic A-scans for further analysis. In order to determine certain time intervals, time gating was applied.

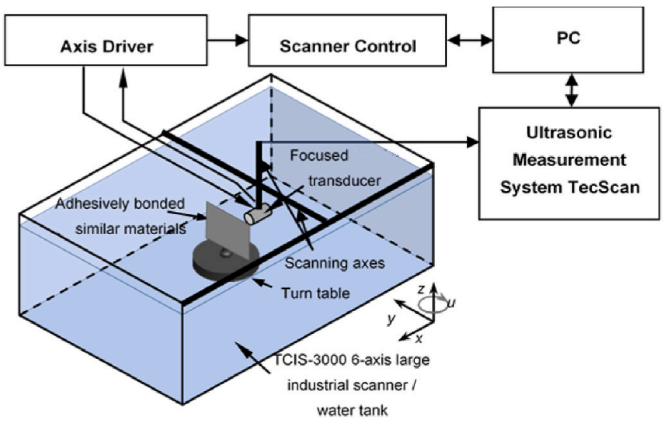

Fig. 3. Experimental set-up of ultrasonic pulse-echo inspection of adhesively bonded aluminium to CFRP.

Implementing time gating to extract only the segments of the signal containing reflections from defects enhances the specificity of the data used for training, as it isolates the critical information required for defect detection The correct determination of the signal segments to be extracted depends on the location of the defects in the sample, the propagation time of ultrasonic waves in aluminium plate and adhesive layer, its thicknesses and the ultrasonic features to be extracted. In this case, interface defects that are located at different depths in the adhesive layer are investigated. Thus, it is necessary to determine the time instances of reflection from interface bonding of the sample.

As it is known, the first reflection received by the sensor is the reflection from the surface of the object. While the initial surface reflection does provide important information about the distance, orientation, and curvature of the sample, in our specific analysis, the focus is on the interface reflections. These interface reflections are more critical for detecting defects within the adhesive layer, as they directly correspond to the bonding interfaces where defects may occur. Therefore, it was decided to extract 2 signal segments from the full signal on A-scans: the time segment of the first interface reflection and the time segment of 3 multiple interface reflections. Analysis of 3 multiple interface reflections is required for extraction of additional ultrasonic features. Signal segments containing multiple repetitive reflections from the interface provide a broader range of data for training the ML model, especially for features extraction requiring analysis of several interface reflections. According to this technique the starting point of the signal as well as the appropriate signal length (from t_1 to t_2 and t_1 to t_3) were determined for further extraction. Extracted time intervals of ultrasonic data are presented in Fig. 5.

2.3.3. Datasets preparation

The next step in data preprocessing for training the ML model is to extract an appropriate amount of defective and not defective data from the sample No 1 that will be used for the training and testing. Selection of defective and not defective data is based on ultrasonic C-scan analysis and A-scans of 2 signal segments extracted – time interval of 1st reflection from the interface (t_1 to t_2) and 3 multiple interface reflections (t_1 to t_3). Firstly, the defective areas corresponding to three defects in all 3 zones were identified. Equivalent-sized non-defective areas were also selected for comparison purposes. In the C-scans, areas representing the perfect bond state were identified through a combination of systematic and manual procedures. Initially, a systematic approach was employed to identify potential areas of perfect bonding. Signal intensity and pattern consistency characteristics were used as a criteria of perfect bond selection. In addition, a manual verification process was conducted. This involves visual inspection of the C-scan images to ensure that selected areas match the expected characteristics of perfect bond such as uniform signal reflection and absence of anomalies. Perfect bond areas were selected by the technician visually from different places between the expected defect areas to cover variability of bond quality, to provide consistency of the data and minimize bias. Hence, 2 separate datasets for each class (defective and not defective) were created. Each class of datasets ensures balanced representation and facilitates supervised learning during ML model training. C-scan images of the 1st reflection from the interface (t_1 to t_2) were generated and utilized to identify areas containing defects and perfect bond for each inspection zone (Fig. 6 (a)). In addition, the same datasets were created for sample No 2 with thick CFRP layer for verification of trained ML model. A C-scan images for the sample No 2 are shown in Fig. 6 (b).

2.3.4. Ultrasonic feature extraction

A comprehensive set of 32 ultrasonic features was extracted from both the defective and non-defective datasets. The features selected were based on our experience of investigation of adhesive bonds and are valid for both samples [4,35]. These extracted features were meticulously cataloged for subsequent utilization in the training of the machine learning model. Ultrasonic features with comprehensive description and

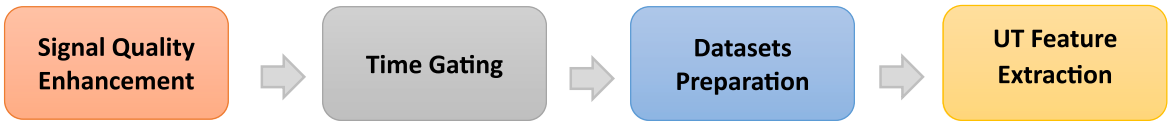

Fig. 4. Steps of data preprocessing.

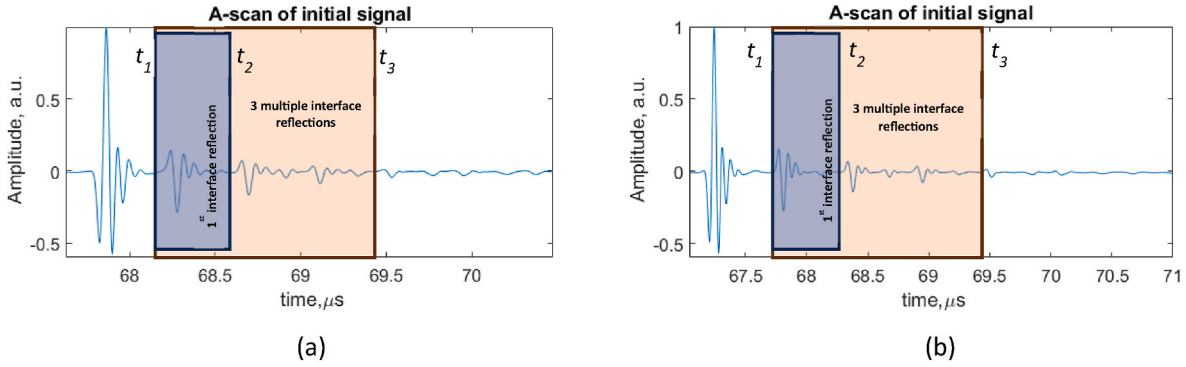

Fig. 5. A-scans of full and extracted signal segments: (a) Sample No 1, (b) Sample No 2.

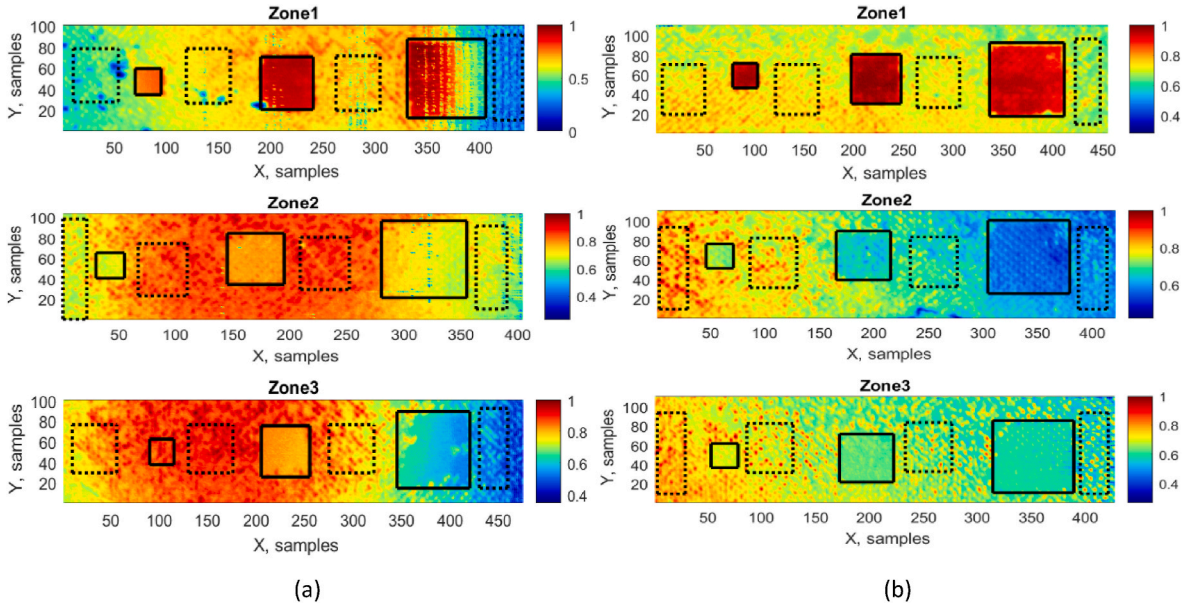

Fig. 6. C-scans with defective areas (solid line) and perfect bond areas (dotted line) identified for extraction: (a) Sample No 1, (b) Sample No 2.

mathematical expressions are presented in Table 1. The features are categorized according to the domains in which they were analyzed: time and frequency.

2.4. Feature engineering

A total of 32 features were extracted from each A-scan, defining time and frequency domain parameters of the ultrasonic signals. While the initial number of features seemed quite large, it complied with the rule of thumb to have at least 10 observations per feature. In our case, a total amount of 54,489 observations represents the total number of A-scans collected from the C-scan image (Fig. 6), corresponding to defective and not defective areas in all 3 zones of the sample. This means that the number of observations (n) was much larger than the number of features (f) $n \gg f$, which is considered sufficient even for models with a higher capacity to overfit. Among the 54,489 observations, 27,159 described the signals measured at defected areas, and 27,330 referenced defect-free areas of the sample under inspection. Among the 27,159 signals measured from defected areas, three subsets of 9053 observations represented "depth 1," "depth 2," and "depth 3" classes, which referenced defects located at different depths.

At this point, we established two datasets that were further used for feature engineering: the first was used for binary classification of "defect" and "no defect" cases, while the second was used for multiclass classification among three classes: "depth 1," "depth 2," and "depth 3." These datasets are further referenced as binary and ternary classifier datasets. The datasets were prepared as two-dimensional data structures ($M \times N$) where rows represent observations and columns represent features. The binary dataset had dimensions of ($n = 54489$, $f = 32$), while the ternary dataset had dimensions of ($n = 27159$, $f = 32$) as it excluded the defect-free measurements.

Each dataset was fed to the feature engineering routine that included

Table 1
List of extracted ultrasonic features.

No	Ultrasonic feature	Assignment		Description	Mathematical expression
		Single interface	Multiple interface		
Time domain					
1	U_{pp}	✓		Peak-to-peak amplitude	$U_{pp} = \max(u(t)) - \min(u(t)),\ t \in t_1 \div t_2$
2	U_{max}	✓		Maximum amplitude	$U_{max} = \max(u(t)), t \in t_1 \div t_2$
3	U_{mean}	✓		Mean amplitude	$U_{mean} = \sum_{i=1}^{N}\left(\frac{u_i(t)}{N}\right),\ t \in t_1 \div t_2.$
4	U_{median}	✓		Median amplitude	$U_{median} = \text{median}\ (u(t)), t \in t_1 \div t_2$
5	U_{sum}	✓		Sum of amplitude value	$U_{sum} = \sum_{i=1}^{N}(u_i(t)),\ t \in t_1 \div t_2$
6	$\|U\|_{sum}$	✓		Absolute sum of amplitude values	$\|U\|_{sum} = \sum_{i=1}^{N}\|u_i(t)\|$
7	A	✓		Absolute Energy	$A = \sum_{t_1}^{t_2} {U_{p-p}}^2$
8	σ	✓		Standard deviation	$\sigma = \sqrt{\frac{1}{N-1}\sum_{i=1}^{N} u_i(t) - \overline{u(t)}}$
9	cv	✓		Variation coefficient	$cv = \frac{\sigma}{u_{mean}}$
10	t_r	✓		Rise time of waveform	$t_r = (i_{end} - i_{start}) \bullet \frac{1}{F_s}$
11	t_f	✓		Fall time of waveform	$t_f = (i_{end} - i_{start}) \bullet \frac{1}{F_s}$
12	S	✓		Waveform symmetry	$S = \frac{t_r}{t_f}$
13	ZCR	✓		Zero-crossing rate	$ZCR = \frac{N_{zc}}{L}$, $N_{zc} = \sum_{n=1}^{N-1}\|\text{sign}(u[n]) - \text{sign}(u[n-1])\|$, N – total number of samples in the signal.
14	CR	✓		Crest factor	$CR = \frac{\|U\|_{max}}{\sqrt{\frac{1}{N}\sum_{i=1}^{N} u_i(t)^2}}$, N – total number of samples in the signal.
15	K_{12}		✓	Ratio coefficient of 1st and 2nd interface reflections	$K_{12} = \frac{U_{pp_1}}{U_{pp_2}}$
16	K_{21}		✓	Ratio coefficient of 2nd and 1st interface reflections	$K_{21} = \frac{U_{pp_2}}{U_{pp_1}}$
17	K_{31}		✓	Ratio coefficient of 3rd and 1st interface reflections	$K_{31} = \frac{U_{pp_3}}{U_{pp_1}}$
18	K_{32}		✓	Ratio coefficient of 3rd and 2nd interface reflections	$K_{32} = \frac{U_{pp_3}}{U_{pp_2}}$
19	Δt_{21}		✓	Absolute time of flight of 2nd and 1st interface reflection	$\Delta t = \|t_2 - t_1\|$
20	Δt_{32}		✓	Absolute time of flight of 3rd and 2nd interface reflection	$\Delta t = \|t_3 - t_2\|$
21	α_{12}		✓	Attenuation comparing 1st and 2nd interface reflection	$\alpha = 20\ log_{10}\frac{U_{pp_1}}{U_{pp_2}}$
22	α_{23}		✓	Attenuation comparing 2nd and 3rd interface reflection	$\alpha = 20\ log_{10}\frac{U_{pp_2}}{U_{pp_3}}$
23	k	✓		Kurtosis	$k = \frac{E(u(t) - \mu)^4}{\sigma^4},\ t \in t_1 \div t_2$
24	s	✓		Skewness	$s = \frac{E(u(t) - \mu)^3}{\sigma^3},\ t \in t_1 \div t_2$
Frequency domain					
25	U_{fmax}	✓		Maximum amplitude	$U_{fmax} = \max(\text{FT}(u(t)),\ t \in t_1 \div t_2$
26	f_{Umax}	✓		Frequency value at the maximum amplitude	$f_{Umax} = \text{argmax}_f\ \text{FT}(u(t)),\ t \in t_1 \div t_2$
27	u_{fmean}	✓		Mean value of the amplitude	$u_{fmean} = \sum_{i=1}^{N}\text{FT}\left(\frac{u_i(t)}{N}\right),\ t \in t_1 \div t_2$
28	σ_f	✓		Standard deviation	$\sigma_f = FT \bullet \sqrt{\frac{1}{N-1}\sum_{i=1}^{N} u_i(t) - \overline{u(t)}}$
29	cv_f	✓		Variation coefficient	$cv_f = \text{FT}\left(\frac{\sigma_f}{u_{fmean}}\right)$
30	f_d	✓		Dominant frequency	$f_d = \frac{\text{idx} \bullet F_s}{L}$
31	s_f	✓		Frequency skewness	$s_f = \frac{E(u(f) - \mu)^3}{\sigma^3}$
32	HNR	✓		Harmonic to noise ratio	$HNR = \frac{E_{harmonic}}{E_{noise}}$, $E_{harmonic} = \sum\|u_h(f)\|^2$, $E_{noise} = \sum\|u_n(f)\|^2$

* u_i- each amplitude value at time t, N – number of observations, $\overline{u(t)}$ – mean value, i_{end} – the index where the signal crosses below the threshold after i_{start}, i_{start} – the index where the signal first exceeds the threshold, F_s – sampling frequency, L – signal length, $u[n]$- signal sample at index n, sign($u[n]$) – the sign of the signal sample, where $(u[n]) = 1$ if $u[n] > 0$, $(u[n]) = -1$ if $u[n] < 0$, $(u[n]) = 0$ if $u[n] = 0$, μ – mean of $(u(t)$, σ is a standard deviation, E is the expected value of the quantity $(u(t) - \mu)^4$ or $(u(t) - \mu)^3$ or $(u(f) - \mu)^3$, FT – Fourier Transform, idx - the index of the maximum magnitude in the Fourier Transform of the signal, $u(f)$ – Fourier Transform of the input signal $u(t)$, $u_h(f)$ – harmonic components in frequency spectrum, $u_n(f)$ – noise components in frequency spectrum.

outlier removal, statistical significance analysis and pairwise correlation analysis. The purpose of this feature engineering was to reduce noise by removing redundant observations and features that carry the same information. Prior to feature engineering in order to ensure feature comparability and prevent numerical instability, all features were scaled to the unit variance according to the expression:

$$z_n = (x_n - \mu) / s, \quad (1)$$

where z_n is the scaled observation x_n, x_n is the n-th observation, μ is the mean of feature column, s is the standard deviation of the feature column, $n = 1 \div N$, where N – is the total number of observations in the feature column.

2.4.1. Outlier removal

The interquartile range (IQR) statistical method was employed to identify and remove extreme values that could potentially skew the results of the machine learning models. In this study, we calculated the IQR as the difference between the 25th and 75th percentiles (IQR = Q_3–Q_1), which separated the lowest 25 % and highest 25 % of the data. To establish the outlier boundaries, we utilized a k factor of 3, setting the outlier boundaries to $\pm 4.7215\sigma$ from the median. Consequently, any observations outside the range [Q_1–k(Q_3–Q_1), Q_3+k(Q_3–Q_1)] were considered outliers. In the case of the binary dataset, outlier detection resulted in the removal of 58 observations, while in the ternary dataset, 7 observations were removed. The remaining datasets had dimensions of ($n = 54431, f = 32$) and ($n = 27152, f = 32$) for the binary and ternary datasets, respectively.

2.4.2. Statistical significance analysis

In this study, the primary aim of the statistical significance analysis was to remove redundant features that do not provide decisive power. For this purpose, we used a two-sample independent *t-test* analysis. This analysis calculates a *t-statistic* based on the difference between the means of two groups and the variability within the groups and compares the result with the critical value of the *t-distribution*. To properly implement the *t-test* analysis, we compared the decisive power of each feature between different classes: "defect" and "no defect" for the binary dataset, and "depth 1," "depth 2," and "depth 3″ for the ternary dataset. We sampled features assigned to each class and iteratively calculated the *t-statistic* for each feature. The null hypothesis for this test was formulated as: there is no significant difference between two subsamples of the same feature that represent different damage states. The p-value was calculated with a confidence interval of 95 %. As a result of the *t-test* analysis, one feature column (symmetry) was removed in the case of the ternary dataset. The remaining feature columns were considered statistically significant and remained in the datasets which had dimensions of ($n = 54431, f = 32$) and ($n = 27152, f = 31$).

2.4.3. Pairwise correlation analysis

To properly handle multicollinearity between features and identify redundant ones, a pairwise correlation analysis was performed. During this analysis, pairwise correlation coefficients were calculated using Pearson correlation as a measure of linear association between all features in the datasets. It is known that correlation analysis without domain knowledge can lead to the removal of features with high predictive power, thus reducing the model's accuracy. To mitigate this issue, we used a similarity threshold of $k = 3$, which allowed us to remove only those features that were correlated with three or more other features. A correlation threshold of 0.75, both for positively and negatively correlated features, was applied. The pairwise correlation analysis revealed that nine features were significantly correlated with more than three other features in the binary dataset and twelve features in the ternary dataset. After removing these correlated features, the binary and ternary datasets had dimensions of ($n = 54431, f = 23$) and ($n = 27152, f = 20$), respectively. The pairwise correlation heatmaps after removal of correlated features are presented in Fig. 7.

In this study, we intentionally didn't perform cross-validation to ensure that feature removal during the correlation analysis did not adversely affect model performance. Instead, we chose a back-propagation approach, where we removed highly correlated features first. After checking the model's performance, we retained the option to reintroduce some features if the performance appeared to be insufficient. The datasets, after pairwise correlation feature removal, were used as the initial datasets for the machine learning analysis. To further explore possibility to reduce data dimension, the dimensionality reduction techniques described in the following chapter were employed.

2.5. Dimensionality reduction

In this section, the dimensionality reduction techniques used to process the binary and ternary datasets presented in the previous section will be briefly discussed. The general aim of this dimensionality reduction is to improve the computational efficiency of the machine learning models, reduce overfitting caused by using models with too many features, and increase the interpretability of the models. This section also aims to find the best balance between the number of features and prediction accuracy, and to identify the most influential features that contribute most to the success of the machine learning model. We used two different approaches for the binary and ternary datasets. For the binary dataset, we subsampled the initial dataset consisting of 32 features based on our a priori knowledge about the features, while for the ternary dataset, we used tree-based, sequential, and recursive feature elimination techniques, as well as linear discriminant analysis (LDA) to transform the data into a low dimensional space. In the following sections, the dimensionality reduction techniques for each dataset will be briefly described, followed by the appropriate results.

2.5.1. Binary dataset

The binary dataset initially consisted of $f = 23$ features and $n = 54431$ observations. To further reduce the data dimensions, we subsampled the initial dataset and created two additional datasets with a reduced number of features. A summary of the selected features is presented in Table 2. As a result, we tested the binary "defect" versus "no defect" classification using three datasets: ($n = 54431, f = 23$), ($n = 52190, f = 16$), and ($n = 54476, f = 7$). The number of observations varied between these datasets due to the outlier removal process, which removed a different number of observations depending on the dataset size. To properly select the features in each dataset, we reviewed the pairwise correlation results and used a priori knowledge about the data. The first dataset with $f = 23$ features included most of the features, including those extracted from a single signal and from subsequent reflections, such as time-of-flight or amplitude ratio. The second dataset, consisting of $f = 16$ features, excluded features measured from two subsequent reflections, containing only those that could be measured from a single reflection in the time and frequency domains. However, it was more complete compared to the last dataset with 7 features, as it included more robust metrics such as waveform rise time, fall time, and zero crossing rate. The final dataset with $f = 7$ features included the minimal number of features, focusing on those found to be most influential in our previous study [35]. Consequently, the binary classifier was tested with these three datasets, as shown in Table 2.

2.5.2. Ternary dataset

The ternary dataset was used for three-class classification – "depth 1," "depth 2," and "depth 3." After feature engineering, the initial ternary dataset consisted of 20 features ($n = 27152, f = 20$), as listed in Table 2. To further decrease the number of dimensions, three dimensionality reduction methods belonging to the feature selection class, namely tree-based, recursive, and sequential, were used. These methods select subsets of features based on different scores. Additionally, a feature transformation technique called linear discriminant analysis

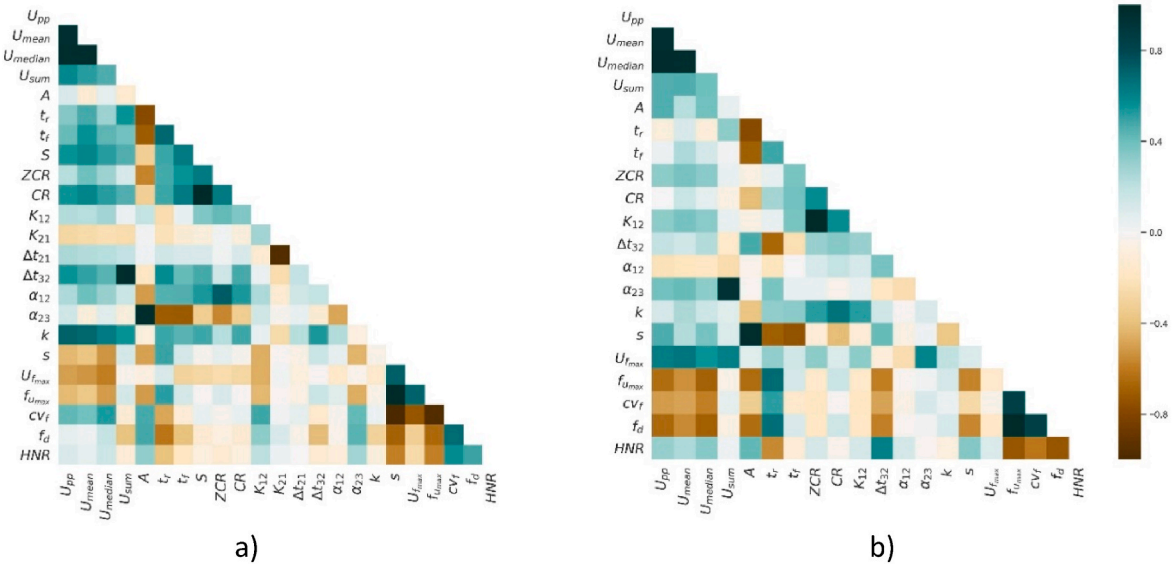

Fig. 7. Heatmaps of binary (a) and ternary (b) datasets after removal of correlated features.

Table 2
Selected features according to binary and ternary classifier datasets.

No.	Ultrasonic feature	Binary classifier			Ternary classifier			
		Initial (f=23)	Single interface (f=16)	Minimised (f=7)	Initial (f=20)	Tree based (f=10)	Recursive (f=19)	Sequential (f=10)
1.	U_{pp}	■	■	■	■	■	■	■
2.	U_{max}							
3.	U_{mean}	■	■		■		■	■
4.	U_{median}	■	■		■		■	■
5.	U_{sum}	■	■		■		■	
6.	$\|U\|_{sum}$							
7.	A	■	■	■	■	■	■	
8.	σ							
9.	cv							
10.	t_r	■	■		■	■	■	
11.	t_f	■	■		■	■	■	■
12.	S	■	■					
13.	ZCR	■	■		■		■	
14.	CR	■	■		■	■	■	■
15.	K_{12}	■			■		■	
16.	K_{21}	■						
17.	K_{31}							
18.	K_{32}							
19.	Δt_{21}	■						
20.	Δt_{32}	■			■		■	
21.	α_{12}	■			■		■	
22.	α_{23}	■			■		■	
23.	k	■	■	■	■			■
24.	s	■	■	■	■		■	
25.	U_{fmax}	■	■	■	■	■	■	■
26.	f_{Umax}	■	■	■	■	■	■	■
27.	u_{fmean}							
28.	σ_f							
29.	cv_f	■	■	■	■	■	■	■
30.	f_d	■			■	■	■	
31.	s_f							
32.	HNR	■	■		■	■	■	■

(LDA) was used to transform multidimensional features into a two-dimensional space.

2.5.2.1. Tree based feature selector. The tree-based feature selector was implemented using an Extra Trees classifier, which is an ensemble learning technique that aggregates the results of multiple de-correlated decision trees and collects the predictions using the majority voting method. This method reduces the risk of overfitting by averaging the results from multiple uncorrelated trees and can also provide the importance scores of the features, enabling a straightforward way to select those features that enhance the model's interpretability and performance [36,37].

To avoid assigning high importance scores to features with low predictive power, we used permutation-based feature importance evaluation. This method measures the decrease in the model score when a single feature is randomly shuffled. Since this evaluation breaks the relation between the feature and the target, the drop in the model score reliably indicates how much the model depends on that particular feature. Additionally, we used a dataset from which correlated features had been removed in the previously described feature engineering section, so the permutation-based feature importance evaluation did not suffer from multicollinearity. In this study, we used 100 tree estimators and 10 permutations for each feature with accuracy scoring and unseen data for feature importance evaluation. As a result, the feature importance scores obtained using the Extra Trees classifier are presented in Fig. 8. The results show that features such as *HNR*, f_d, f_{Umax}, U_{fmax}, *CR*, t_f, t_r, and *A* show high importance and can be considered as the most influential according to the tree-based selector. This feature selection approach removed half of the initial features, and the subset of 10 features with the highest importance scores was used as a separate dataset for damage depth classification ($n = 27152$, $f = 10$). The features kept after tree-based selector are summarized in Table 2.

2.5.2.2. Recursive feature selector. Recursive dimensionality reduction is a backward selection technique that iteratively removes the least important features and re-evaluates the model's performance [38,39]. For this purpose, we used the Extra Trees classifier as the core model due to its compatibility with backward selection approach. This model was first trained with all features, and then at each step, we removed one feature and retrained the model using the reduced number of features to evaluate its performance. To define the stopping criteria, we implemented a 3-fold cross-validation estimator that finds the optimal number of features by comparing scores of different subsets. The average cross-validation accuracy score versus the number of selected features for the recursive feature selector is presented in Fig. 9 (a). The results in Fig. 9 (a) demonstrate that the recursive feature selector selected 19 features removing only the kurtosis feature as shown in Table 2.

Although this feature removal technique has some disadvantages, such as evaluating the features mostly independently without considering their interaction and the selected subsets strongly depending on the chosen model, it was only one of the few dimensionality reduction techniques employed in this study. Therefore, we accepted its limitations.

2.5.2.3. Sequential feature selector. Another feature selection technique that we implemented in this study was the sequential feature selector. Unlike the recursive feature selector, this method requires defining the number of remaining features beforehand. The sequential feature selector aims to find the optimal number of features by sequentially adding or removing features in a forward or backward direction. In this study, we used a forward feature selector, starting with an empty set of features and sequentially evaluating all features that could be added to the current dataset. The stopping criterion was set to 10 features, meaning that half of the features were to be eliminated. We used 5-fold cross-validation to evaluate the model's performance with the current subset. Although the greedy approach is known to not always find the optimal subset of data, as it makes decisions based only on the current subset, it was part of a larger group of dimensionality reduction methods. Its advantages, such as simplicity, improved model efficiency, and helping to avoid overfitting, outweighed its limitations. The average cross-validation accuracy score versus the number of selected features for the sequential feature selector is presented in Fig. 9 (b). The results of the sequential feature selector show that among the 10 selected features, none were associated with data that includes multiple signal reflections within the damaged area, such as amplitude ratio and time of flight. It also selected all the features indicated as most influential by the tree-based feature selector (see Fig. 8), except for f_d. However, the sequential selector showed a higher preference for magnitude-based features such as U_{mean} and U_{median}. The features selected by sequential feature selector are presented in Table 2.

2.5.2.4. LDA feature selector. Finally, LDA was the last technique in the dimensionality reduction approaches used in this study. LDA is commonly employed to transform multi-dimensional feature datasets into low-dimensional data by maximizing the means and minimizing the variance between different classes by using Fischer's approach [40,41].

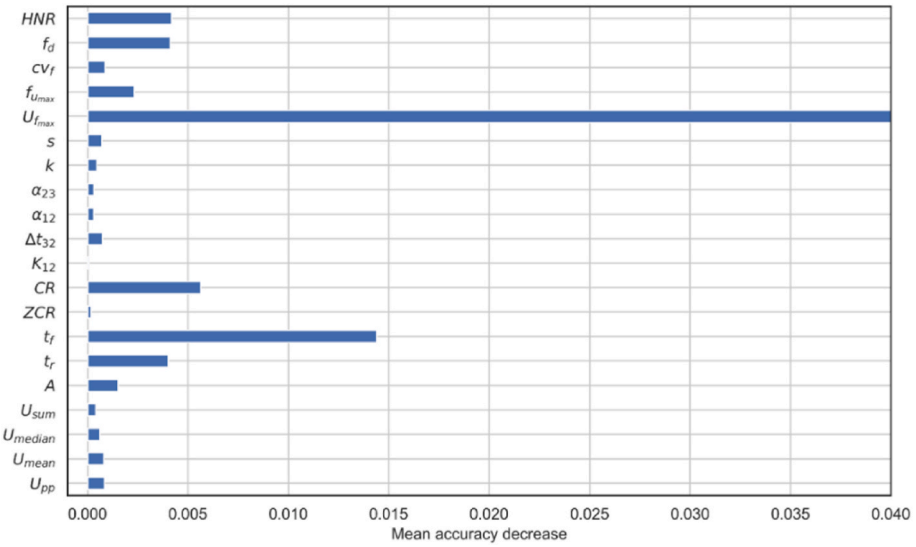

Fig. 8. Permutation based importance of the features in the ternary dataset calculated using Extra trees classifier.

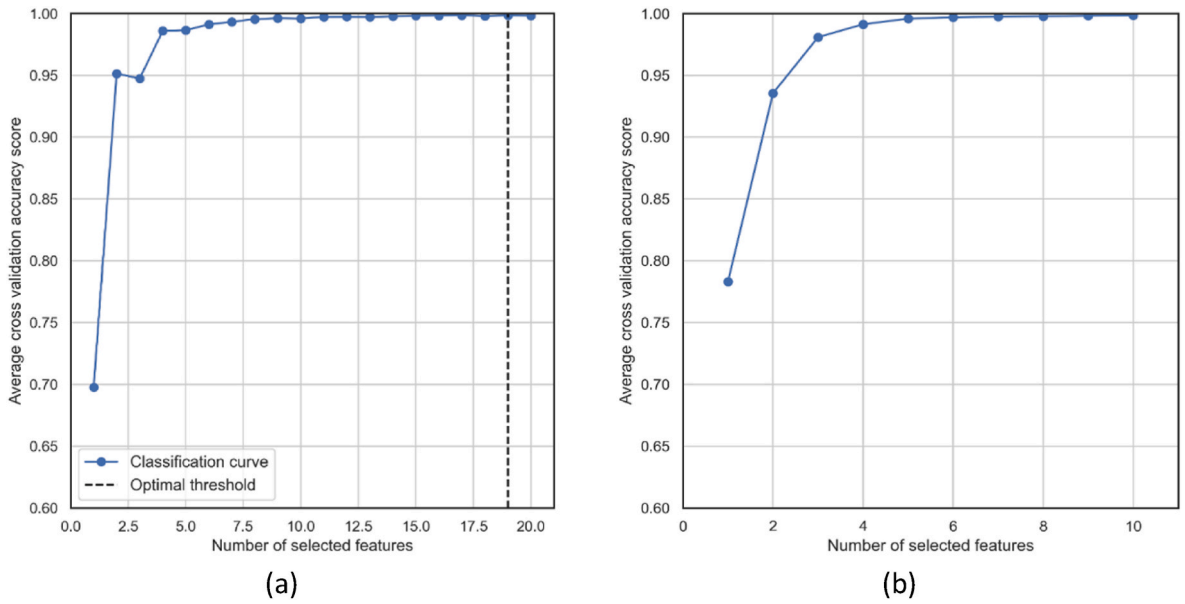

Fig. 9. Average cross-validation accuracy score versus the number of selected features for recursive (a) and sequential (b) feature selectors.

In this way, instances belonging to different classes are separated, and in most cases depending on the number of classes, can be visualized to gain a better insight into the class boundaries. While LDA itself is commonly used as a classification technique, the dimensionality reduction is inherently performed by LDA as part of the process as it seeks to find linear combinations of the original features that best separate the classes. Hence it can be used as supervised technique to reduce the number of features. In a typical use case, since we initially had $k = 3$ classes, with LDA we retained 2 dimensions (k–1). During the LDA analysis we assumed that the classes area is linearly separable and has the same statistical distribution within class. The representation of the ternary dataset in the 2D space after applying linear discriminant analysis as a dimensionality reduction technique is presented in Fig. 10. The explained variances for the first two LDA components were 85 % and 14 %, respectively. The results suggest that the "depth 1" class can be separated well from the "depth 2" and "depth 3" classes, while the latter two classes slightly overlap, indicating that some of the "depth 3" data will be misclassified as "depth 2" and vice versa.

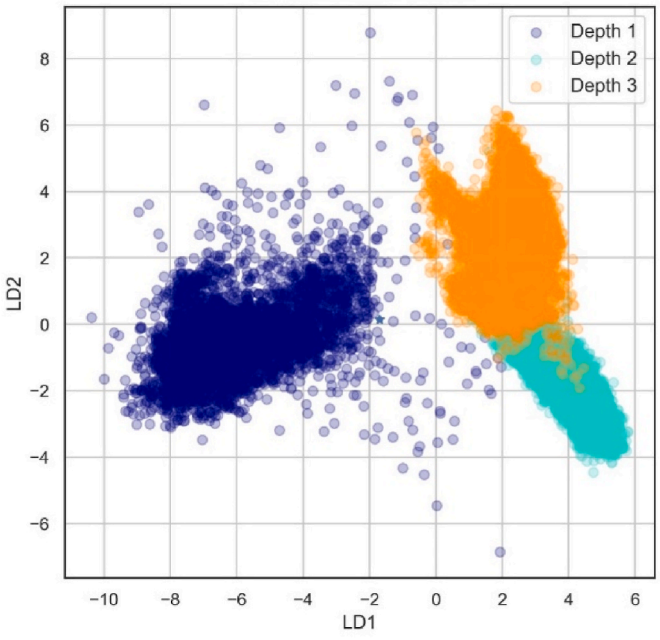

Fig. 10. Ternary dataset in the 2D space after applying linear discriminant analysis.

As it can be seen from the data in Table 2, the features that included multiple reflections within the defect (K_{21}, K_{31}, K_{32}, Δt_{21}, Δt_{32}, α_{12}, α_{23}) were kept only in the initial and the recursive datasets. The tree-based selector also dismissed the magnitude-related features, keeping only U_{pp} and A. The features from the ternary dataset that were retained across all subgroups were U_{pp}, t_f, CR, U_{fmax}, f_{Umax}, cv_f, and HNR, showing a good correlation with the feature importance scores presented in Fig. 8. Additionally, features such as U_{mean}, U_{median}, A, t_r, and f_d were selected by 3 out of 4 feature selectors.

3. Results and discussion

As presented in the previous section, our initial goal was to predict both "defect" and "no defect" cases and the depth of the defect by classifying them as "depth 1", "depth 2" and "depth 3", depending on where the delamination is located. We started with a dataset of 32 features and performed feature engineering, including outlier removal, statistical significance analysis, and pairwise correlation analysis. After these steps, we were left with datasets consisting of 23 features for the binary classifier ("defect" and "no defect") and 20 features for the ternary classifier ("depth 1", "depth 2" and "depth 3"). These feature sets were considered as the starting point datasets.

To further reduce the number of dimensions, we subsampled the binary dataset, creating two additional datasets consisting of 16 and 7 features, respectively. Hence, we had a total of 3 datasets for binary classification. For the ternary dataset, we employed various dimensionality reduction techniques such as tree-based, recursive, sequential, and LDA feature selectors. This process resulted in 5 datasets for ternary classification. All these datasets were trained and evaluated independently.

For this purpose, each dataset was randomly split into training and testing sets, with 65 % of the data for training and 35 % for testing. To maintain the same number of observations within separate classes, we used stratified splitting with 5-fold cross-validation. For classification, we used a support vector machine (SVM) classifier, which seeks to find the optimal hyperplane that best differentiates the classes while allowing for some misclassifications by providing a soft margin. The SVM

classifier was implemented using a one-versus-rest approach, where $n^*(n\text{-}1)/2$ (n is the number of classes) classifiers were constructed for each combination of pairwise classes. The hyperparameter tuning of the SVM model was performed before fitting it to the data, which suggested using a linear kernel function. Each model was trained on the described datasets. Then, the pretrained models were evaluated on unseen data, which was extracted from sample No 2, on which an independent measurement was performed. The unseen data was prepared in the same way as the original training/testing data, meaning that both feature and observation removal routines were performed. The results between different datasets and on train/test and unseen data are presented in a form of confusion matrix **C**, where **C**0,0 is the fraction of true negatives, **C**1,0 – false negatives, **C**1,1 – true positives and **C**0,1 – false positives. The accuracy score in the confusion matrix shows a fraction of correctly and incorrectly classified observation.

The results of the binary "defect" versus "no defect" classifiers for the train/test and unseen data are presented in Figs. 11 and 12. The outcomes of the confusion matrices for the train/test data represent the highest classification accuracy for the initial dataset of features (n = 54431, f = 23) which is higher than 90 % for both - the true positive and true negative outcomes. The single interface dataset (n = 52190, f = 16) with a reduced number of features also shows high prediction accuracy with a slight decrease in the true positive rate. However, in the case of minimised dataset (n = 54476, f = 7) there is still high accuracy observed for the "no defect" classification (96 %), but quite significant reduction for the true positive rate where only 73 % of the "defect" cases were correctly identified. In the context of non-destructive testing in aerospace industry which demands extremely high safety standards and regulations, the sensitivity should be as close to 100 % as possible to ensure all defects are detected. Therefore, true positive rate of 73 % is insufficient in this field. The results received for the unseen data of different object (sample No 2) are close to train/test data. Confusion matrices of initial and single interface datasets display quite high classification accuracies, while a significant drop of true positive rate (74 %) is observed for the minimised dataset as well. Nevertheless, the results of classification accuracy of unseen data in comparison to trained/test data indicates that the created machine learning models are highly effective for application in defect detection in adhesive joints.

The results of ternary classification ("depth 1", "depth 2" and "depth 3") for train/test and unseen data are presented in Fig. 13 and Fig. 14. Confusion matrices of 5 datasets of dimensionality reduction (initial (f = 20), tree based (f = 10), recursive (f = 19), sequential (f = 10), and LDA) display the classification accuracy values. As a result, for the train/tests data ternary classification accuracy is quite high and mostly very close to 100 % in the case of all 5 feature subsets. This means that the depth of the defect location in the adhesive zone of the object can be determined accurately using the trained model.

For unseen data extracted from the sample used for testing and verification only, the outcomes of confusion matrices show the larger variance. The highest classification accuracy of "depth 1" and "depth 3" shows the following feature subsets: LDA, recursive and initial. In addition, classification accuracy of "depth 1" is higher than 95 % for all feature subsets. The best result of "depth2" prediction is observed using sequential feature subset which is 80 %. It was most difficult to classify between "depth 2" and "depth 3" in the case of initial, tree based and recursive feature subsets. The minimum value of correctly identified "depth 2" cases is 57 %, and the maximum value of mistakenly identified "depth 2" as "depth 3" is 32 %. However, the classification accuracy of "depth 2" is not less than 57 % except for LDA feature subset, where true positive rate is only 35 % while the remaining cases identified as "depth 1". With respect to all 3 depths classification, best performance shows initial and recursive datasets.

Fig. 6 shows the C-scans for Zone 2 and Zone 3, which correspond to areas with interface defects located in the middle of the adhesive layer "depth 2" and between the adhesive and the CFRP layer "depth 3", respectively. The amplitude contrast between the defective and non-defective areas is minimal, resulting in a significantly lower detectability of interface defects in these zones compared to Zone 1. In these zones, distinguishing defective shapes and edges was also challenging. For Zone 3 of the sample with the thin CFRP plate, the smallest defect could not be identified experimentally. These limitations could influence the ML model training leading to reduced classification accuracy for the ternary dataset on unseen data and resulting in confusion between "depth 2" and "depth 3".

In this study, we intentionally chose to use a classic machine learning approach with SVMs over more sophisticated neural networks. Our decision was driven by the simplicity and transparency of the resulting classification. While the features were handpicked rather than selected by the model, their selection was based on our previous research [4,35], which demonstrated their effectiveness in debonding detection. As a result, this paper establishes a direct link between the features, their importance, and the classification's sensitivity and specificity, providing new insights. Additionally, it's well known that SVMs with well-understood features can generalize effectively on unseen data and avoid overfitting. By demonstrating the model's predictions on data that was not used in the training process and was obtained from a sample with different geometry and during an independent experiment, we confirmed the model's ability to generalize.

On the other hand, advanced neural networks may capture patterns that might elude even researchers with expertise in the field. For this reason, deep learning techniques could be explored in future work to automate feature extraction, potentially improve classification performance, and increase the method's robustness outside controlled laboratory conditions, making it more adaptable to industrial environments. Nonetheless, we believe the approach demonstrated in this study significantly enhances defect detection accuracy compared to previous methods that relied solely on post-processing algorithms to improve interface defect detectability [4,16]. These ML models enabled us to

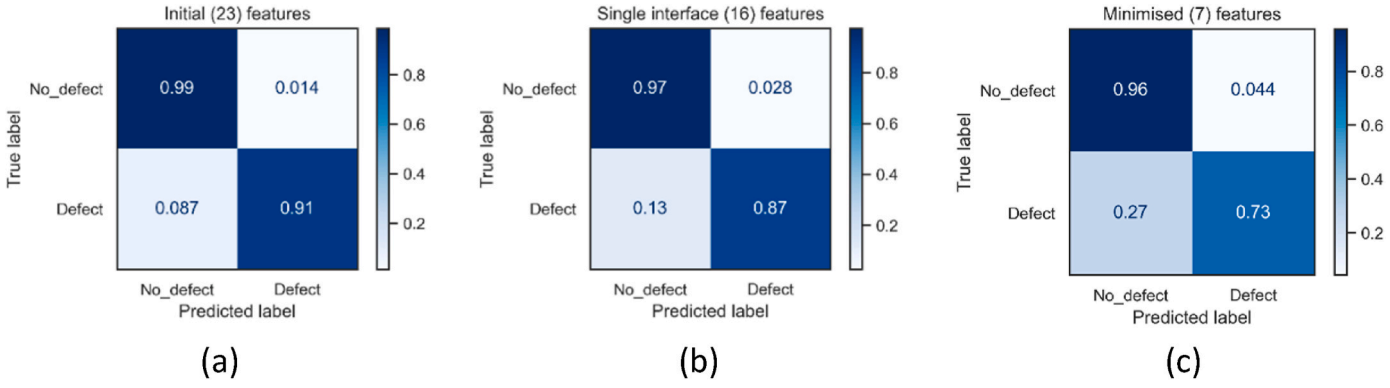

Fig. 11. Confusion matrices of binary classification for train/test data: (a) initial feature subset, (b) single interface subset, and (c) minimised feature subset.

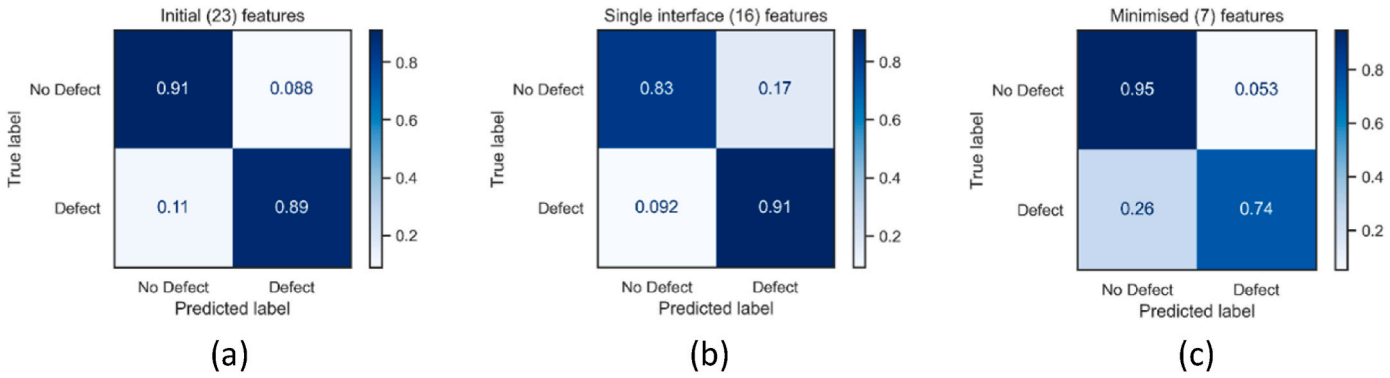

Fig. 12. Confusion matrices of binary classification for unseen data: (a) initial feature subset, (b) single interface subset, and (c) minimised feature subset.

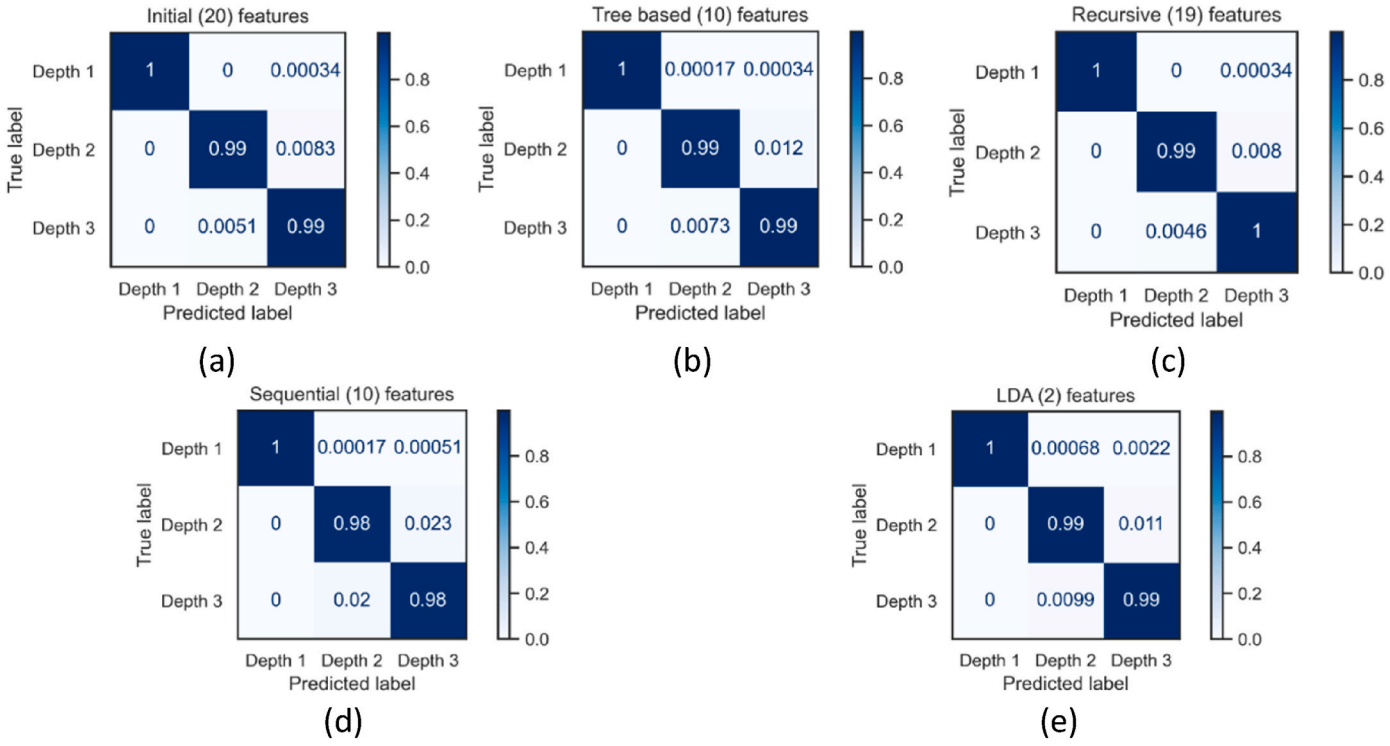

Fig. 13. Confusion matrices of ternary classification for train/test data: (a) initial feature subset, (b) tree - based, (c) recursive, (d) sequential, (e) LDA.

achieve a high accuracy in identifying defect depths, which was previously unattainable, particularly due to the challenges posed by very thin layers of adhesive and adherends, leading to signal overlap.

4. Conclusion

In this study, a semi-automated technique based on ultrasonic pulse echo method and machine learning algorithms has been developed to detect interface defects in adhesive joints and classify them according to their depth location in the adhesive layer. Adhesively bonded aluminium to CFRP joints with disbond type defects located at different depth in adhesive were analyzed. In the data preprocessing stage, the signal quality was effectively improved ensuring that extracted features were relevant and robust for classification tasks. Thirty-two ultrasonic features from the whole and time gated signal of single and multiple interface reflections were performed to capture essential signal characteristics related to defect detection.

The developed ML model automatically and successfully detected and classified defects according to their depth locations. Thus, the ML-based approach demonstrates the potential of combining ultrasonic techniques with machine learning for precise defect identification in adhesive joints and composite materials. The analysis included both binary and ternary classifier datasets, with feature selection and dimensionality reduction techniques applied to optimize the ML models. The main results of the ML model performance evaluation are as follows.

1. The study confirmed that U_{pp}, t_f, CR, U_{fmax}, f_{Umax}, cv_f, and HNR features which were retained across all subgroups have a highest importance score for accurate defect classification. In addition, according to Extra Trees classifier high importance score has A, t_r, and f_d features which were retained in 3 out of 4 feature selectors.
2. The highest “defect” vs. “no defect” classification accuracy for the binary datasets was observed for the initial and single interface feature subsets. For the train/test data, the classification accuracy is greater than 90 % for the initial subset and higher than 87 % for the single interface subset. For unseen data, the classification accuracy slightly decreased but remained higher than 83 % for true negative and 89 % for true positive rates.

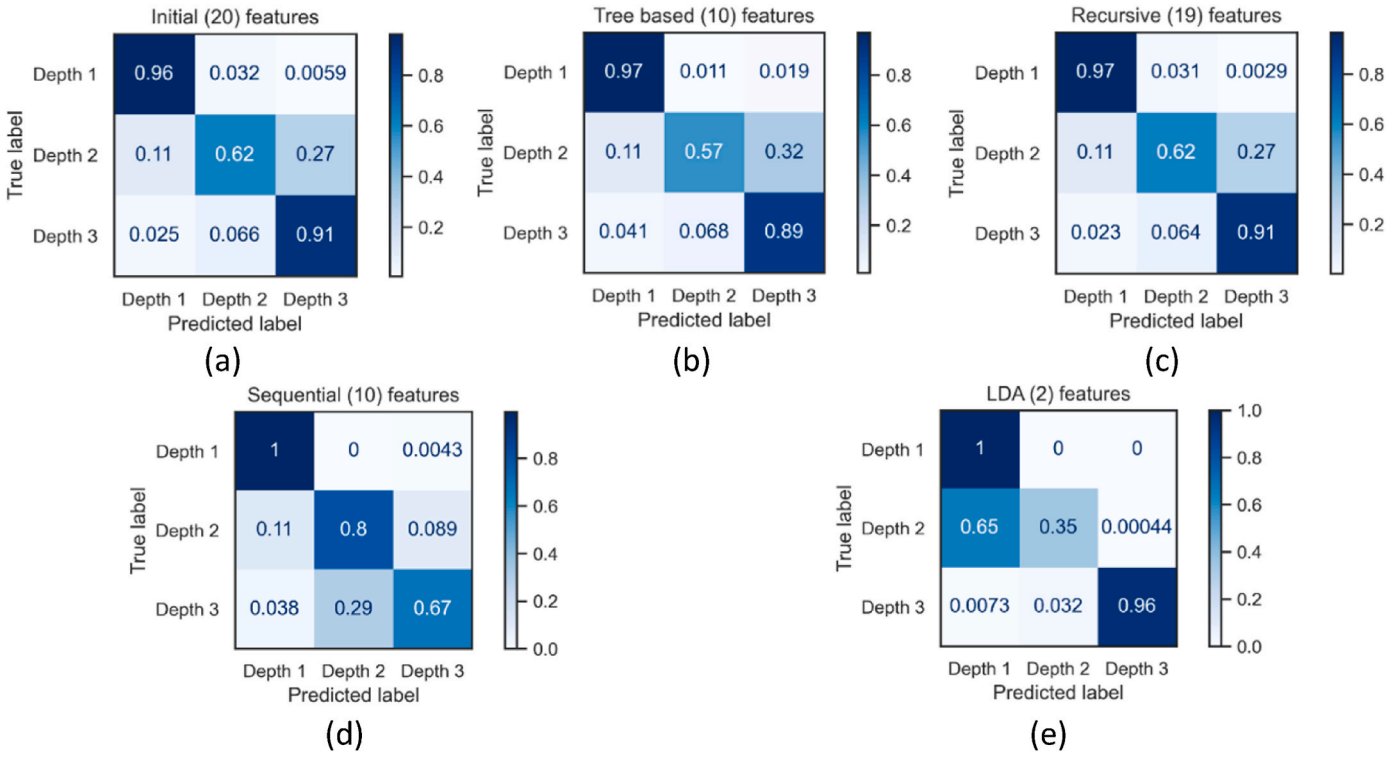

Fig. 14. Confusion matrices of ternary classification for unseen data: (a) initial feature subset, (b) tree based, (c) recursive, (d) sequential, (e) LDA.

3. The highest accuracy for ternary classification taking into account all 3 depths ("depth 1", "depth 2" and "depth 3") was observed in all 5 confusion matrices of feature subsets which is greater than 98 %. However, for the unseen data the highest classification accuracy shows that initial and recursive feature subsets which contain features of multiple reflections are more reliable. These subsets correctly classified "depth 1″ in more than 96 % of cases, "depth2" in more than 62 % of cases, and "depth3" in 91 % of cases.
4. "Depth 2" is in the middle of the adhesive zone, while "depth 3" is at the bottom, making them more challenging to separate. The misclassification of "depth 2" as "depth 3" was due to low amplitude contrast in Zone 2 and Zone 3 (Fig. 6) making defect distinction difficult compared to Zone 1; blurred defect edges, signal overlap due to thin layers and complex structure as well as experimental identification limitation of the smallest defect in Zone 3.

Despite the fact that today's modern neural networks can also perform the same classification task on the same dataset, the conventional SVM-based machine learning approach described offers significant practical advantages, particularly in terms of training speed and ease of implementation, making it more financially viable. In comparison, neural networks can require several days to several weeks to be trained depending on the task complexity. Furthermore, for classification tasks such as "defect" vs. "no defect" and defect depth localization ("depth1", "depth2", "depth3"), the Support Vector Machine is straightforward and user-friendly. This simplicity enhances its applicability in research for further analysis and testing across various types of adhesive joints and interface defects as well as widespread use in related industries for defect detection and localization, and process automation. However, as the complexity and size of data increases, SVM approach performance can be limited compared to neural networks, which are designed to handle large datasets and can model complex nonlinear relationships. NNs can automatically extract features and offer greater potential for generalisation and robustness, especially when dealing with real-world variability and noise.

The combination of ultrasonic techniques with ML offers a powerful and cost-effective tool for semi-automated defect detection and classification in adhesive joints. Nevertheless, the incorporation of deep learning techniques in future studies could further optimize these results.

CRediT authorship contribution statement

Damira Smagulova: Writing – review & editing, Writing – original draft, Visualization, Validation, Software, Methodology, Investigation, Funding acquisition, Formal analysis, Data curation. **Vykintas Samaitis:** Writing – review & editing, Writing – original draft, Visualization, Validation, Supervision, Software, Project administration, Methodology, Formal analysis, Data curation, Conceptualization. **Elena Jasiuniene:** Writing – review & editing, Supervision, Project administration, Methodology, Investigation, Funding acquisition, Conceptualization.

Declaration of competing interest

The authors declare that they have no known competing financial interests or personal relationships that could have appeared to influence the work reported in this paper.

Data availability

Data will be made available on request.

Acknowledgment

This research was supported by the Research Council of Lithuania (LMTLT), agreement no. S-PD-22-25 and agreement no. S-MIP-22-5.

References

[1] Yao K, Li X, Lu Z. Study on ultrasonic quantitative evaluation technique based on BP neural network and D-S evidence theory. Ultrasonics 2024;138:107235. https://doi.org/10.1016/j.ultras.2023.107235.

[2] Tenreiro AFG, Ramalho GMF, Lopes AM, da Silva LFM. Advances in structural adhesive bonding. In: Structural monitoring of adhesive joints using machine learning. second ed. 2023. https://doi.org/10.1016/B978-0-323-91214-3.00033-8.
[3] Solodov I, Kornely M, Philipp J, Stammen E, Dilger K, Kreutzbruck M. Linear vs nonlinear ultrasonic testing of kissing bonds in adhesive joints. Ultrasonics 2023; 132:106967. https://doi.org/10.1016/j.ultras.2023.106967.
[4] Smagulova D, Yilmaz B, Jasiuniene E. Ultrasonic features for evaluation of adhesive joints: a comparative study of interface defects. Sensors 2024:24–176. https://doi.org/10.3390/s24010176.
[5] Yamaguchi Y, Sato Y. Simultaneous nondestructive estimation of thickness and longitudinal wave velocity of adhesive layers in adhesive joints through air-coupled ultrasonic testing. NDT E Int 2023;138:102905. https://doi.org/10.1016/j.ndteint.2023.102905.
[6] Rao J, Yang F, Mo H, Kollmannsberger S, Rank E. Quantitative reconstruction of defects in multi-layered bonded composites using fully convolutional network-based ultrasonic inversion. J Sound Vib 2023;542:117418. https://doi.org/10.1016/j.jsv.2022.117418.
[7] Wei Y, Jin X, Luo Q, Li Q, Sun G. Adhesively bonded joints – a review on design, manufacturing, experiments, modeling and challenges. Composites Part B 2024; 276:111225. https://doi.org/10.1016/j.compositesb.2024.111225.
[8] Titov SA, Maev RG, Bogachenkov AN. Pulse-echo NDT of adhesively bonded joints in automotive assemblies. Ultrasonics 2008;48:6–7. https://doi.org/10.1016/j.ultras.2008.07.001.
[9] Jodhani J, Handa A, Gautam A, Ashwni Rana R. Ultrasonic non-destructive evaluation of composites: a review. Mater Today Proc 2023;78:627–32. https://doi.org/10.1016/j.matpr.2022.12.055.
[10] Crane RL, Hart-Smith J, Newman J. Adhesive bonding: science, technology and applications. second ed., vol. 8. Nondestructive inspection of adhesive bonded joints; 2021. p. 215–56. https://doi.org/10.1016/B978-0-12-819954-1.00008-3.
[11] Jasiūnienė E, Mažeika L, Samaitis V, Cicėnas V, Mattsson D. Ultrasonic non-destructive testing of complex titanium/carbon fibre composite joints. Ultrasonics 2019;95:13–21. https://doi.org/10.1016/j.ultras.2019.02.009.
[12] Markatos DN, Pantelakis SG, Tserpes KI. Comprehensive structural integrity. In: The effect of contamination-generated defects on the mechanical performance of adhesively bonded joints. second ed., vol. 2. Destructive and Non-Destructive Assessment; 2023. p. 810–33. https://doi.org/10.1016/B978-0-12-822944-6.00014-1.
[13] He C, Li Y, Lyu Y, Song G, Wu B. Ultrasonic reflection characteristics of FRP-to-FRP bonded joints with thick adhesive layers for bonding evaluation: theoretical analysis. Compos Struct 2020;246:112402. https://doi.org/10.1016/j.compstruct.2020.112402.
[14] Fame CM, Wu C, Feng P, ho Tam L. Numerical investigations on the damage tolerance of adhesively bonded pultruded GFRP joints with adhesion defects. Compos Struct 2022;301:116223. https://doi.org/10.1016/j.compstruct.2022.116223.
[15] Nicassio F, Cinefra M, Scarselli G, Filippi M, Pagani A, Carrera E. Numerical approach to disbonds in bonded composite single lap joints: comparison between carrera unified formulation and classical finite element modeling. Thin-Walled Struct 2023;188:110813. https://doi.org/10.1016/j.tws.2023.110813.
[16] Smagulova D, Mazeika L, Jasiuniene E. Novel processing algorithm to improve detectability of disbonds in adhesive dissimilar material joints. Sensors 2021;21(9): 3048. https://doi.org/10.3390/s21093048.
[17] Brotherhood CJ, Drinkwater BW, Dixon S. The detectability of kissing bonds in adhesive joints using ultrasonic techniques. Ultrasonics 2003;41(7). https://doi.org/10.1016/S0041-624X(03)00156-2.
[18] Li Y, Yao K, Li X. An ultrasonic signal reconstruction algorithm of multilayer composites in non-destructive testing. Appl Acoust 2022;186:108461. https://doi.org/10.1016/j.apacoust.2021.108461.
[19] Haldren H, Yost WT, Perey D, Elliott Cramer K, Gupta MC. A constant-frequency ultrasonic phase method for monitoring imperfect adherent/adhesive interfaces. Ultrasonics 2022;120:106641. https://doi.org/10.1016/j.ultras.2021.106641.
[20] Li Z, Xiao L, Qu W, Lu Y. Local defect internal resonance method for ultrasonic damage identification of adhesive interface debonding. Int J Non Lin Mech 2023; 157:104541. https://doi.org/10.1016/j.ijnonlinmec.2023.104541.
[21] Wojtczak E, Rucka M. Damage imaging algorithm for non-destructive inspection of CFRP/steel adhesive joints based on ultrasonic guided wave propagation. Compos Struct 2022;297:115930. https://doi.org/10.1016/j.compstruct.2022.115930.
[22] Ghose B, Panda RS, Balasubramaniam K. Guided A0 wave mode interaction with interfacial disbonds in an elastic-viscoelastic bilayer structure. NDT E Int 2021; 124:102543. https://doi.org/10.1016/j.ndteint.2021.102543.
[23] Spytek J, Ziaja-Sujdak A, Dziedziech K, Pieczonka L, Pelivanov I, Ambrozinski L. Evaluation of disbonds at various interfaces of adhesively bonded aluminum plates using all-optical excitation and detection of zero-group velocity Lamb waves. NDT E Int 2020;112:102249. https://doi.org/10.1016/j.ndteint.2020.102249.
[24] Kumar S, Sunny MR. A novel nonlinear Lamb wave based approach for detection of multiple disbonds in adhesive joints. Int J Adhesion Adhes 2021;107:102842. https://doi.org/10.1016/j.ijadhadh.2021.102842.
[25] Pyzik P, Ziaja-Sujdak A, Spytek J, O'Donnell M, Pelivanov I, Ambrozinski L. Detection of disbonds in adhesively bonded aluminum plates using laser-generated shear acoustic waves. Photoacoustics 2021;21:100226. https://doi.org/10.1016/j.pacs.2020.100226.
[26] Roth W, Giurgiutiu V. Structural health monitoring of an adhesive disbond through electromechanical impedance spectroscopy. Int J Adhesion Adhes 2017;73. https://doi.org/10.1016/j.ijadhadh.2016.11.008.
[27] Ehrhart B, Valeske B, Bockenheimer C. Non-destructive evaluation (NDE) of polymer matrix composites. Non-destructive evaluation (NDE) of aerospace composites: methods for testing adhesively bonded composites 2013. https://doi.org/10.1533/9780857093554.2.220 [Chapter 9].
[28] Chen CH. Encyclopedia of materials: science and technology. second ed.). NDT: Role of Artificial Intelligence and Neural Networks; 2001. p. 5994–6. https://doi.org/10.1016/B0-08-043152-6/01050-0.
[29] Prakash N, Nieberl D, Mayer M, Schuster A. Learning defects from aircraft NDT data. NDT E Int 2023;138:102885. https://doi.org/10.1016/j.ndteint.2023.102885.
[30] Chen D, Zhou Y, Wang W, Zhang Y, Deng Y. Ultrasonic signal classification and porosity testing for CFRP materials via artificial neural network. Mater Today Commun 2022;30:103021. https://doi.org/10.1016/j.mtcomm.2021.103021.
[31] Guo C, Ren J, Xu J, Bai L. Ultrasonic defect characterization using Bayesian inversion and scattering matrix denoising neural networks. NDT E Int 2023;136: 102813. https://doi.org/10.1016/j.ndteint.2023.102813.
[32] Tunukovic V, McKnight S, Pyle R, Wang Z, Mohseni E, Gareth Pierce S, Vithanage RKW, Dobie G, MacLeod CN, Cochran S, O'Hare T. Unsupervised machine learning for flaw detection in automated ultrasonic testing of carbon fibre reinforced plastic composites. Ultrasonics 2024;140:107313. https://doi.org/10.1016/j.ultras.2024.107313.
[33] Li J, Gopalakrishnan K, Piao G, Pacha R, Walia P, Deng Y, Chakrapani SK. Classification of adhesive bonding between thermoplastic composites using ultrasonic testing aided by machine learning. Int J Adhesion Adhes 2023;125: 103427. https://doi.org/10.1016/j.ijadhadh.2023.103427.
[34] Fu LL, Yang JS, Li S, Luo H, Wu JH. Artificial neural network-based damage detection of composite material using laser ultrasonic technology. Measurement 2023;220:113435. https://doi.org/10.1016/j.measurement.2023.113435.
[35] Samaitis V, Yilmaz B, Jasiuniene E. Adhesive bond quality classification using machine learning algorithms based on ultrasonic pulse-echo immersion data. Journal of Sound and Vibratoin 2023;546:117457. https://doi.org/10.1016/j.jsv.2022.117457.
[36] Aggarwal CC. Data classification: algorithms and applications. first ed. Chapman and Hall/CRC; 2014. https://doi.org/10.1201/b17320.
[37] Pedregosa F, et al. Scikit-learn: machine learning in Python. J Mach Learn Res 2011. https://doi.org/10.48550/arXiv.1201.0490.
[38] Pal M, Foody GM. Feature selection for classification of hyperspectral data by SVM. IEEE Trans Geosci Rem Sens 2010;48(5). https://doi.org/10.1109/TGRS.2009.2039484.
[39] El Mountassir M, Yaacoubi S, Ragot J, Mourot G, Maquin D. Feature selection techniques for identifying the most relevant damage indices in SHM using Guided Waves. 8th European Workshop On Structural Health Monitoring (EWSHM 2016), e-Journal of Nondestructive Testing; vol. 21(8). https://www.ndt.net/?id=20151.
[40] Tharwat A, Gaber T, Ibrahim A, Hassanien AE. Linear discriminant analysis: a detailed tutorial. AI Communications 2017;30:169–90. https://doi.org/10.3233/AIC-170729.
[41] Zhu F, Gao J, Yang J, Ye N. Neighborhood linear discriminant analysis. Pattern Recogn 2022;123:108422. https://doi.org/10.1016/j.patcog.2021.108422.